Theoretical study of C_2 and C_2^-: $X\,^1\Sigma_g^+$, $a\,^3\Pi_u$, $X\,^2\Sigma_g^+$, and $B\,^2\Sigma_u^+$ potentials

Jeffrey A. Nichols[a] and Jack Simons
Chemistry Department, University of Utah, Salt Lake City, Utah 84112

(Received 13 January 1987; accepted 27 February 1987)

We employ multiconfigurational self-consistent field and multiconfigurational electron propagator methods to characterize the $X\,^2\Sigma_g^+$ and $B\,^2\Sigma_u^+$ states of C_2^- and the $X\,^1\Sigma_g^+$ and $a\,^3\Pi_u$ states of C_2 over a wide range of bond lengths (1.0–1.9 Å). We find a systematic difference of approximately 0.3 eV in the *relative* positioning of our anion- and neutral-state potentials compared to the anion–neutral spacing in the best curves constructed from experimental data. Once this energy shift is taken into consideration, all four of our computed potential energy curves are in reasonably good agreement with experimental information. However, there remains a substantial difference in the relative positioning of our $B\,^2\Sigma_u^+$ and $a\,^3\Pi_u$ curves, compared to the best available experimental data, at larger bond lengths. The relevance of this discrepancy and of our other data to the present state of experimental knowledge on C_2^-/C_2 is discussed.

I. INTRODUCTION

A. Experimental studies of C_2/C_2^-

There are very few molecular anions which possess bound electronically excited states. C_2^- is such a species and is the most widely experimentally studied[1] molecular anion possessing bound excited states which are optically accessible.

The lowest electronic state of C_2^- is the $X\,^2\Sigma_g^+$ state. Two bound electronically excited states have been positively identified[2–4]: the $A\,^2\Pi_u$ and $B\,^2\Sigma_u^+$ states. There is speculation[5] that two additional states of $^4\Sigma_u^+$ and $^4\Delta_u$ symmetry could also be found in the same spectral regions as the established bound states. In this same region, two electronic states of the neutral C_2 species can also be found[6,7]: the $X\,^1\Sigma_g^+$ and the $a\,^3\Pi_u$ states. All of these C_2^- and C_2 states lie within approximately 4 eV of one another. The physical origin of these closely spaced levels is well known[8] to lie in the near degeneracy of the partially filled $2\sigma_u$, $3\sigma_g$, $1\pi_u$ and $1\pi_g$ molecular orbitals, all of which have orbital energies which are slightly negative (i.e., they are bound orbitals in the Koopmans' theorem sense). The latest experimental placement[9] of these states and their *dominant* electronic configurations are given in Fig. 1 and Table I, respectively. It is important to note from Table I that the $C_2^-\,X\,^2\Sigma_g^+ \rightarrow C_2\,X\,^1\Sigma_g^+ + e^-$ and the $C_2^-\,X\,^2\Sigma_g^+ \rightarrow C_2\,a\,^3\Pi_u + e^-$ electron detachment processes are predominantly one-electron transitions whereas the $C_2^-\,B\,^2\Sigma_u^+ \rightarrow C_2\,X\,^1\Sigma_g^+ + e^-$ and the $C_2^-\,B\,^2\Sigma_u^+ \rightarrow C_2\,a\,^3\Pi_u + e^-$ detachments represent two-electron transitions. We wish to stress this important difference between detachments from $X\,^2\Sigma_g^+\,C_2^-$ and $B\,^2\Sigma_u^+\,C_2^-$ because we make use of these differences in this paper to generate a rigorous test of our computational method and to demonstrate that our method is capable of treating one- and two-electron transitions in a balanced manner.

Leading spectroscopists have produced a large body of data[1–4,6,7] from which much of the electronic structure of the C_2^-/C_2 systems can be deduced. The relevant C_2^- data began with the 1968 flash-absorption experiment[2] of Herzberg and Lagerqvist. Since 1968, several additional experiments have been carried out, some giving direct $C_2^- \rightarrow C_2$ energy splittings and others yielding indirect results. Because the present state-of-the-art $X\,C_2 \rightarrow X\,C_2^-$ electron affinity (EA) depends on both direct and indirect measurements, we give below a very brief outline of how the EA of C_2 has evolved, and we chronicle the various experimental studies of C_2 and C_2^- which pertain to the present study.

As mentioned previously, initial identification of the C_2^- X and B states was made in 1968 by Herzberg and Lagerqvist.[2] The best direct measurement of the EA of C_2 came shortly thereafter with Feldman's work[6] in 1970. Using low resolution photodetachment spectroscopy, Feldman ob-

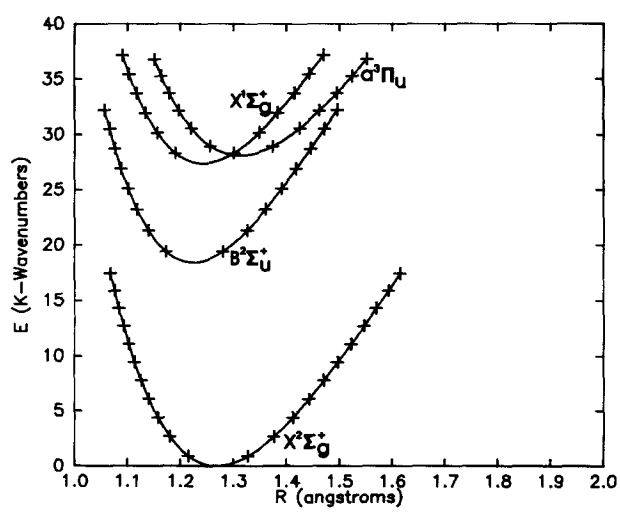

FIG. 1. Potential energy curves for the X and B states of C_2^- and the X and a states of C_2 reproduced from the best experimental data (vibrational level turning points) obtained from Lineberger and co-workers (Ref. 9). The + marks indicate the vibrational levels.

[a] Permanent address: Chemistry Department, Malone College, Canton, Ohio.

 0021-9606/87/126972-10$02.10

TABLE I. Relevant C_2 and C_2^- electronic states and their dominant configurations.

Species	State	Dominant configuration
C_2^-	$X\,^2\Sigma_g^+$	$KK\ 2\sigma_g^2 2\sigma_u^2 1\pi_u^4 3\sigma_g^1$
C_2^-	$A\,^2\Pi_u$	$KK\ 2\sigma_g^2 2\sigma_u^2 1\pi_u^3 3\sigma_g^2$
C_2^-	$B\,^2\Sigma_u^+$	$KK\ 2\sigma_g^2 2\sigma_u^1 1\pi_u^4 3\sigma_g^2$ for $r<1.5$ Å
		($KK\ 2\sigma_g^2 2\sigma_u^2 1\pi_u^3 3\sigma_g^1 1\pi_g^1$ at $r>1.5$ Å)
C_2^-	$^4\Sigma_u^+$	$KK\ 2\sigma_g^2 2\sigma_u^2 1\pi_u^3 3\sigma_g^1 1\pi_g^1$
C_2^-	$^4\Delta_u$	$KK\ 2\sigma_g^2 2\sigma_u^2 1\pi_u^3 3\sigma_g^1 1\pi_g^1$
C_2	$X\,^1\Sigma_g^+$	$KK\ 2\sigma_g^2 2\sigma_u^2 1\pi_u^4$
C_2	$a\,^3\Pi_u$	$KK\ 2\sigma_g^2 2\sigma_u^2 1\pi_u^3 3\sigma_g^1$

tained a value of 3.54 ± 0.05 eV for the adiabatic $X\,C_2 \rightarrow X\,C_2^-$ EA. Further refinements of this value have subsequently been made based upon reinterpretation of Feldman's data and less direct measurements (e.g., two-photon photodetachment spectroscopy). In 1972, Lineberger and Patterson,[4] using two-photon photodetachment spectroscopy, observed initial (i.e., one photon) $X \rightarrow B\ C_2^-$ electronic excitation followed by subsequent photodetachment from the B excited state. In 1980 Jones *et al.*[7] used single-photon photodetachment methods to look at a series of strong resonances in the photodetachment spectrum of C_2^- caused by absorption from $X\,^2\Sigma_g^+\ C_2^-$ to various vibrational levels of $B\,^2\Sigma_u^+$ followed by autodetachment of the B state of C_2^-. In particular, photon-induced transitions from high-lying vibrational levels ($v = 6$–10) of $X\,^2\Sigma_g^+\ C_2^-$ to the $v = 5$–8 levels of $B\,^2\Sigma_u^+\ C_2^-$ were observed to yield subsequent autodetachment from the $B\,^2\Sigma_u^+$ levels. A very important result of Jones *et al.* was that the $v = 5$ level of the $B\,^2\Sigma_u^+$ state of C_2^-, even for heavy carbon (^{13}C), underwent autodetachment. The $X\,^2\Sigma_g^+\ (v=0) \rightarrow B\,^2\Sigma_u^+\ (v=5)$ transition energy thus places a stringent *upper bound* on the EA;$EA(C_2) \leqslant 3.408$ eV. This value is in contradiction with Feldman's earlier EA of 3.54 ± 0.05 eV. Jones *et al.*, in reinterpreting Feldman's original data, argue that the sharp onset in Feldman's photodetachment cross section is inconsistent with producing $X\,^1\Sigma_g^+\ C_2$ plus a p-wave outgoing electron. In contrast, production of the $a\,^3\Pi_u\ C_2$ state and an s-wave electron would yield the observed sharp onset. Therefore, Jones *et al.* argue that Feldman's detachment onset must correspond to the opening of the $C_2\ a\,^3\Pi_u + e^-$ continuum and that his EA is, therefore, too high by the difference in the $v = 0$ levels of the $C_2\ X\,^1\Sigma_g^+$ and the $a\,^3\Pi_u$ states—a difference of 0.08 eV. Jones *et al.* also argue that more realistic error bars of $+0.15$ and -0.10 eV should be assigned to Feldmann's cross-section onset because of rotational broadening and contributions from excited negative ion vibration. In summary, Feldman's data has been reinterpreted to give EA $(C_2) = 3.46(+0.15, -0.10)$. The autodetachment-based *upper bound* to the EA is thus found to lie within these error bars.

A *lower bound* to the EA lies in another important result of Jones *et al.* They found a factor of at least 10 in the autodetachment rates of the $v = 5$ and $v = 6$ levels of $B\,^2\Sigma_u^+\ C_2^-$. After considering several possibilities, Jones *et al.* concluded that the best interpretation of this fact places the $v = 5$ level of $B\,^2\Sigma_u^+\ C_2^-$ above the $v = 0$ level of $X\,^1\Sigma_g^+\ C_2$ and below the $v = 0$ level of a $^3\Pi_u\ C_2$. Autodetachment from $B\,^2\Sigma_u^+$ ($v = 5$) to $X\,^1\Sigma_g^+$ ($v = 0$) is thus energetically possible but slow because this is a two-electron transition (see configuration lists in Table I). Population of the $v = 6$ level of $B\,^2\Sigma_u^+\ C_2^-$ is then postulated to open up the $v = 0$ level of $C_2\ a\,^3\Pi_u + e$. This $B\,^2\Sigma_u^+\ (v=0) \rightarrow a\,^3\Pi_u\ (v=0)$ autodetachment can proceed by a one-electron transition at large R (see Table I) as a result of which the autodetachment rate dramatically increases. These interpretations of the relative positioning of $v = 5$ and 6 $B\,^2\Sigma_u^+$ and $v = 0\ X\,^1\Sigma_g^+$ and $v = 0\ a\,^3\Pi_u$ give a *lower bound* to the C_2 EA of 3.374 eV. The net result is that the current experimental value for C_2's EA is $3.374\ \text{eV} \leqslant EA(C_2) \leqslant 3.408$ eV.

B. Theoretical studies

A great deal of theoretical effort has been devoted to characterizing the C_2/C_2^- system, in particular to calculating the C_2 electron affinity. Significant earlier studies include the self-consistent field (SCF) calculations of Cade and Wahl[10] and the SCF and configuration interaction (CI) calculations of Barsuhn.[11] Later, more sophisticated calculations appeared including the Hartree–Fock-limit SCF study and CI calculations of Dupuis and Liu,[8] multireference double-excitation CI (MRD CI) calculations by Zeitz, Peyerimhoff, and Buenker,[5,12] multiconfigurational SCF-self-consistent electron pair (MCSCF-SCEP) calculations by Rosmus and Werner,[13] and Green's function calculations by Cederbaum, Domcke, and von Niessen.[14]

The early SCF calculations incorrectly ordered the low-lying states of both the C_2^- anion and the C_2 neutral.[12] The addition of electron correlation corrected the ordering of the states and thus gave proper assignments of the ground states. An excellent analysis of the features which are necessary for accurately computing the EA of C_2 has been given by Dupuis and Liu.[8] In particular, their electron density contour plots of the $2\sigma_u$ and $3\sigma_g$ orbitals of C_2 indicated a large amount of spatial overlap between these two orbitals. This, in turn, explained why the $2\sigma_u$, $3\sigma_g$, $1\pi_u$, and $1\pi_g$ orbitals all play essential roles in the configuration mixing and electron correlation of C_2 and C_2^-. Dupuis and Liu found an electronic correlation *contribution* to the electron affinity of C_2 equal to -0.79 eV (i.e., this is the difference between their HF-limit RHF EA of 4.33 ± 0.02 eV and Feldman's experimental EA of 3.54 ± 0.05 eV). Using the updated experimental EA of 3.374–3.408 discussed earlier (for the remainder of this paper we will take 3.400 eV to be the best adiabatic experimental EA), we arrive at -0.93 eV for the correlation contributions to C_2's EA. Notice that the SCF EA is actually *larger* than the correct EA, which implies that the correlation energy of C_2 is *larger* than that of C_2^-. This is another unusual characteristic of the C_2/C_2^- system. Dupuis and Liu explored several different levels of CI (e.g., single, double, and quadruple excitations from one- and two-configuration reference functions) to obtain theoretical estimates of the EA. They obtained EA's ranging from 2.84 to 3.75 eV and concluded that calculating the EA of C_2 accurately is extremely difficult.

More recent calculations—the MRDCI results of Zeitz *et al.*[5,12] and the MCSCF-SCEP results of Rosmus and Werner[13]—yielded several very accurate predictions of spectroscopic constants which are within experimental error for the low-lying states of the C_2^- anion and the low-lying states of the C_2 neutral molecule. However, even these calculations experienced difficulty placing the C_2^- states *relative* to the C_2 neutral states and hence in determining the adiabatic C_2 EA.

The goal of the present work was to address the particular difficulties of the C_2 EA and the characterization of the lowest few potential energy curves of C_2 and C_2^- using multiconfigurational Green's function methods. As previously indicated, the experimental determination of the EA of C_2 is critically dependent upon the potential curves of $X\,^1\Sigma_g^+$, $a\,^3\Pi_u$ C_2, and $B\,^2\Sigma_u^+$ C_2^-. In the calculations reported here the two electronic states of the anion pertinent to the autodetachment process, the X and B states, are *both* used as reference states in MCEP calculations from which the energy differences to the two relevant neutral states, the X and a states, are determined. In this way, we are able to achieve additional support for the quality both of the EA we predict and of the potential curves we obtain.

II. MCEP DEVELOPMENTS AND CALCULATIONAL DETAILS

A. Overview of MCEP methodology

The multiconfigurational electron propagator (MCEP) formalism[15] has been derived, tested, and applied in several earlier publications. It yielded ionization potentials to within a few tenths of an eV of established experimental values for valence, inner valence, and shakeup ionizations of three well known yet difficult test cases: N_2, O_2, and F_2. The MCEP method differs from other Green's function approaches[16] in that it is not a perturbation-theory-based method but rather utilizes a multiconfigurational reference state and a multiconfigurational ionization-operator manifold. This renders the method very suitable for computing ionization energies of highly correlated and/or open-shell systems.

The one-electron propagator which the MCEP calculates has been shown[17] to be block diagonal in the total spin quantum numbers (S,M) when the normal spin–orbital creation a_i^+ and destruction a_j operators are replaced by the following spin-adapted creation and destruction operators u^+,u and d^+,d:

$$\begin{aligned} u_{r\beta}(S,M) &= -(S+M+1)a_{r\beta} + a_{r\alpha}S^+, \\ u_{r\beta}^+(S,M) &= -(S+M)a_{r\beta}^+ + a_{r\alpha}^+S^-, \\ d_{r\beta}(S,M) &= (S-M)a_{r\beta} + a_{r\alpha}S^+, \\ d_{r\beta}^+(S,M) &= (S-M+1)a_{r\beta}^+ + a_{r\alpha}^+S^-. \end{aligned} \tag{1}$$

Here S and M are quantum numbers labeling the S^2 and S_z eigenvalues of the reference state containing N electrons $|0;NSM\rangle$, and $S^\pm$ are the spin raising and lowering operators. The one-electron propagator is thus factored into two noninteracting propagators resulting in ion states which are pure spin states.

In the MCEP method, the exact reference state from which electron removal or addition occurs is approximated by a complete-active-space MCSCF (CAS-MCSCF) state. The exact operator manifold is approximated by all possible single electron removal or addition operators and all possible single electron removal or addition operators coupled to ket–bra operators mapping the reference state $|0;NSM\rangle$ into all possible MCSCF orthogonal complement states $|\Gamma;NSM\rangle$ (the orthogonal complement space consists of all members of the CAS configuration space which are orthogonal to $|0;NSM\rangle$).

The two resulting noninteracting multiconfigurational electron propagators are the so-called up propagator ($G^{\rm up}$; which yields $N-1$ electron states of spin $S+\frac{1}{2}$, $M+\frac{1}{2}$, and $N+1$ electron states of spin $S-\frac{1}{2}$, $M-\frac{1}{2}$) and the down propagator ($G^{\rm down}$; which yields $N-1$ electron states of spin $S-\frac{1}{2}$, $M+\frac{1}{2}$ and $N+1$ electron states of spin $S+\frac{1}{2}$, $M-\frac{1}{2}$). The corresponding operator manifolds for $G^{\rm up}$ are

$$\begin{aligned} &\{u_{r\beta}(S,M),\ u_{r\beta}(S,M)|\Gamma;NSM\rangle\langle 0;NSM|, \\ &d_{r\beta}(S+1,M)|\Gamma;N(S+1)M\rangle\langle 0;NSM|, \\ &|0;NSM\rangle\langle\Gamma;N(S-1)M|d_{r\beta}(S-1,M),\ \text{and} \\ &|0;NSM\rangle\langle\Gamma;NSM|u_{r\beta}(S,M)\}, \end{aligned} \tag{2}$$

and for $G^{\rm down}$ they are

$$\begin{aligned} &\{d_{r\beta}(S,M),\ d_{r\beta}(S,M)|\Gamma;NSM\rangle\langle 0;NSM|, \\ &u_{r\beta}(S-1,M)|\Gamma;N(S-1)M\rangle\langle 0;NSM|, \\ &|0;NSM\rangle\langle\Gamma;N(S+1)M|u_{r\beta}(S+1,M), \\ &|0;NSM\rangle\langle\Gamma;NSM|d_{r\beta}(S,M)\}. \end{aligned} \tag{3}$$

Here the $|\Gamma;NS'M\rangle$ refers to a state in the orthogonal complement space of the MCSCF reference state $|0;NSM\rangle$. Within the Green's function method, ionization energies are obtained by solving the generalized eigenvalue problem

$$|\mathsf{A} - E\mathsf{S}| = 0, \tag{4}$$

where

$$A_{ij} = (h_i|\hat{H}|h_j) = \langle 0;NSM|\{h_i^+,H,h_j\}|0;NSM\rangle \tag{5}$$

and

$$S_{ij} = (h_i|h_j) = \langle 0;NSM|\{h_i^+,h_j\}|0;NSM\rangle. \tag{6}$$

The operators h_i are elements of the operator manifold, described above in Eqs. (2) and (3), and the brackets { } denote the usual anticommutators of Green's function theory.

The inclusion of all elements in such operator manifolds quickly becomes unmanageable for typical calculations with neutral reference states. For anion studies, the use of extended atomic orbital basis sets gives rise to even larger operator manifolds. We have therefore found it essential to develop an operator screening procedure to limit the number of operators used in any calculation. The operator space described above is known to be over complete.[15(a)] The *redundant* operators can be identifed by examining the metric matrix (S) and can then be transformed out of the eigenvalue problem of Eq. (4). In past MCEP calculations,[15] further reduction of the operator space was introduced by employing an energy criterion involving the orbital energies and

Hamiltonian expectation values of the complement states. Such criteria are counterproductive in applications which employ a large number of diffuse atomic basis functions (e.g., in anion or Rydberg state studies because the low-energy molecular orbitals (MOs) are *not* the most important orbitals for correlating the occupied (core or valence) orbitals. The low-energy MOs describe diffuse weakly bound or unbound charge density with little to no amplitude in the valence region. The virtual orbitals needed for proper electron correlation are often higher in energy as a result of which criteria which utilize only orbital energies can not be used.

In this paper, we introduce what we believe is a more reasonable and efficient criterion for limiting the operator manifold. In order to generate potential curves using the MCEP method, a consistent (i.e., over a wide range of internuclear distances) systematic selection of the most important operators is needed. The selection process which we utilized begins by identifying a dominant ionization operator (denoted P) of either the orbital ionization type (u or d) or the ket–bra ionization (i.e., shakeup) type (e.g. $u|\Gamma\rangle\langle 0|$). For each such dominant ionization, a search is made among all of the other operators (denoted Q). The relative "importance" of each operator is measured by the square of the A–ES matrix element coupling that operator to the dominant operator $[(P|\hat{H}|Q)-E(P|Q)]^2$, divided by the (approximate) energy difference between these two states $(Q|\hat{H}|Q)-E(Q|Q)$, with the energy parameter E taken at $(P|\hat{H}|P)/(P/P)$. This perturbation-like estimate of the coupling between operators Q and the primary operator P is very similar to what is used in configuration selection/screening procedures in large scale CI calculations.[18] Such a scanning procedure is computationally fast since only diagonal terms in the secondary operator space must be evaluated. This operator manifold screening process was used in all of the calculations reported in the next section. As with any selection procedure, a cutoff tolerance is involved. If this tolerance is set to be very small, essentially all operators are included in our manifold, but the screening is therefore useless. Therefore, a compromise needs to be reached between choosing too tight a tolerance and including too few operators. We believe that our cutoff tolerance is reasonable because it results in substantial reduction in the operator manifold while yielding only small fluctuations in the computed electron detachment energies as the bond length R is varied (note the small oscillations present in our numerical data in Figs. 2 and 3).

B. Further calculational details

1. Atomic orbital basis set

In carrying out the calculations whose results are described below we focused on *both* of the C_2^- states which played important roles in the resonance studies of Jones *et al.*, the $X\,^2\Sigma_g^+$ and $B\,^2\Sigma_u^+$ states. Our choice of atomic basis set and the partitioning of the molecular orbitals into core, active and unoccupied orbitals needed to be flexible enough to handle both of these states as well as the $X\,^1\Sigma_g^+$ and $a\,^3\Pi_u$ states of C_2.

The basis set which we employed consisted of the standard Dunning[19] $5s4p$ contraction (from which previous calculations using MC reference states of neutral molecules have had good success) plus a single polarization[20] d orbital whose exponent (0.63) was optimized for the energy of the ground state carbon atom. To accommodate the more extended charge density expected in the anion C_2^- states, a diffuse s orbital with exponent 0.023 and a diffuse p orbital with exponent 0.034 (as suggested by Dunning and Hay[21]) were also added. This resulted in a contracted Gaussian basis set of $6s5p1d$ on each carbon atom for a total of 54 basis functions. We view this as a "chemically decent" basis set rather than one which is capable of addressing electron correlation to a very high accuracy (i.e., better than 0.3 eV). Exactly this kind of basis was very successfully used in earlier MCEP studies[15] of the ionization potentials of F_2, N_2, and O_2. We explored the merit of enhancing this basis by carrying out several MCSCF and MCEP calculations with various larger bases. Even a basis having $8s$, $6p$, and $1d$ orbitals plus $1s$ and $1p$ diffuse functions was found not to yield either substantially more accurate (compared to the best available experimental and theoretical data) MCSCF energies or detachment energies than those obtained with the basis we finally chose to use.

2. MCSCF reference states

Rosmus and Werner[13] had good success in characterizing the lowest three anion states of C_2^- using the MCSCF-SCEP method. Upon examination of the dominant electronic configurations which appear in their wave functions, we were able to generate a similar configuration space within our CAS-MCSCF picture by using a particular partitioning of the molecular orbitals into core, active, and unoccupied orbitals. We used a core subspace of $1\sigma_g^2 1\sigma_u^2 2\sigma_g^2$ and the following active orbitals $2\sigma_u, 3\sigma_g, 3\sigma_u, 1\pi_u$, and $1\pi_g$. All of the other molecular orbitals were taken as unoccupied. This selection of seven active orbitals (the $1\pi_u$ and $1\pi_g$ orbitals are degenerate) containing seven electrons resulted in 104 $^2\Sigma_g^+$ configurations and 104 $^2\Sigma_u^+$ anion configurations, which were then used in our MCSCF calculations for the $X\,^2\Sigma_g^+$ and $B\,^2\Sigma_u^+$ states of C_2^-.

The $X\,^1\Sigma_g^+$ and $a\,^3\Pi_u$ C_2 potential energy curves of neutral C_2 were generated from *both* the $X\,^2\Sigma_g^+$ and $B\,^2\Sigma_u^+$ MCSCF states of C_2^- using the MCEP method outlined earlier. In Table I, the principal electronic configurations for these anion and neutral states are listed. It should be pointed out again that ionizations from the $X\,^2\Sigma_g^+$ C_2^- MCSCF reference to either the $X\,^1\Sigma_g^+$ or $a\,^3\Pi_u$ C_2 states are predominantly one-electron in nature. In contrast, the ionizations from the $B\,^2\Sigma_u^+$ C_2^- MCSCF reference to $X\,^1\Sigma_g^+$ or $a\,^3\Pi_u$ are predominantly two-electron or shakeup type transitions. In Table II, the *primary* operators which are needed in the ionization operator manifolds for the various ionizations are given.

III. RESULTS AND DISCUSSIONS

A. Anion and neutral potential curves

In Fig. 2 we display our MCSCF-computed C_2^- $X\,^2\Sigma_g^+$ potential curve along with the corresponding $X\,^2\Sigma_g^+$ curve

TABLE II. Primary ionization operators for the various MCEP electron detachment transitions.

Transition	Type	Primary operator
$X\,^2\Sigma_g^+ (S=\frac{1}{2}, M=-\frac{1}{2}) \xrightarrow{G^{\text{down}}} X\,^1\Sigma_g^+ (S=0, M=0)$	one-electron	$d_{3\sigma_g}$
$X\,^2\Sigma_g^+ (S=\frac{1}{2}, M=\frac{1}{2}) \xrightarrow{G^{\text{up}}} a\,^3\Pi_u (S=1, M=1)$	one-electron	$u_{1\pi_u}$
$B\,^2\Sigma_u^+ (S=\frac{1}{2}, M=-\frac{1}{2}) \xrightarrow{G^{\text{down}}} X\,^1\Sigma_g^+ (S=0, M=0)$	two-electron	$d_{1\pi_g\vert^2\Pi_g\rangle\langle 0\vert}$[a]
$B\,^2\Sigma_u^+ (S=\frac{1}{2}, M=\frac{1}{2}) \xrightarrow{G^{\text{up}}} a\,^3\Pi_u (S=1, M=1)$	two-electron	$u_{1\pi_u\vert X\,^2\Sigma_g^+\rangle\langle 0\vert}$

[a] $|^2\Pi_g\rangle$ is the state with the following dominant configurations: $KK\ 2\sigma_g^2 2\sigma_u^2 \pi_u^4 \pi_g^1$ and $KK\ 2\sigma_g^2 3\sigma_g^2 \pi_u^4 \pi_g^1$.

inferred from experimental data[9] on C_2^-'s vibrational/rotational energy level patterns. Also shown are the $C_2\ X\,^1\Sigma_g^+$ and $a\,^3\Pi_u$ curves which we obtain by adding our MCEP-computed electron detachment energies to our $X\,^2\Sigma_g^+$ energies. The "experimental" $X\,^1\Sigma_g^+$ and $a\,^3\Pi_u$ curves are also shown.

In Fig. 3, we display both our MCSCF-computed and the experimental $C_2^-\ B\,^2\Sigma_u^+$ potential energy curves over a wide range of bond lengths plus the MCEP and experimental $C_2\ X\,^1\Sigma_g^+$ and $a\,^3\Pi_u$ curves. In this case, the theoretical C_2 potentials were obtained by adding our MCEP-computed detachment energies to our $B\,^2\Sigma_u^+$ energies.

In Figs. 4 and 5, we show experimental and theoretical $C_2\ X\,^1\Sigma_g^+$ and $a\,^3\Pi_u$ energy curves in which both of the theoretical curves have been energy-shifted to force their $X\,^1\Sigma_g^+$ minima to coincide with the experimental minima (they have not been shifted along the R axis). The pairs of theoretical curves shown in Figs. 4 and 5 correspond to data generated by adding our MCEP detachment energies to either our $X\,^2\Sigma_g^+$ or our $B\,^2\Sigma_u^+$ MCSCF state energies. As Fig. 4 clearly demonstrates, the *shape* of our $X\,^1\Sigma_g^+$ potential (as derived either from our $X\,^2\Sigma_g^+$ or our $B\,^2\Sigma_u^+$ energies) is in excellent agreement with the potential inferred from experimental data. Our $a\,^3\Pi_u$ potentials shown in Fig. 5 are in reasonable agreement with the experimental potential except that the equilibrium bond lengths seem to differ by approximately 0.03 Å. The agreement in the shapes of our $a\,^3\Pi_u$ potentials and the experimental curve is emphasized in Fig. 6 where the equilibrium bond lengths are shifted to coincide.

The graphical descriptions of our C_2 and C_2^- potential energy curves contained in Figs. 2–6 support the following conclusions:

(i) The shapes and equilibrium bond lengths of our $X\,^2\Sigma_g^+$ and $B\,^2\Sigma_u^+$ potentials are in excellent agreement with the experimental curves.

(ii) The MCEP-computed energy differences between the neutral $X\,^1\Sigma_g^+$ and $a\,^3\Pi_u$ potentials and our anion potentials seem to be offset by approximately 0.3 eV (see Figs. 7 and 8). That is, our computed detachment energies seem to be too small by approximately 0.3 eV. The need for a systematic shift in our computed ion-neutral energy *differences* to achieve excellent overlap with the experimental $C_2^-\ X\,^2\Sigma_g^+$ and $C_2\ X\,^1\Sigma_g^+$ potentials arises, in our opinion, from errors in our computed EAs of approximately 0.3 eV. Errors in computed EAs of this magnitude, even within the best state-

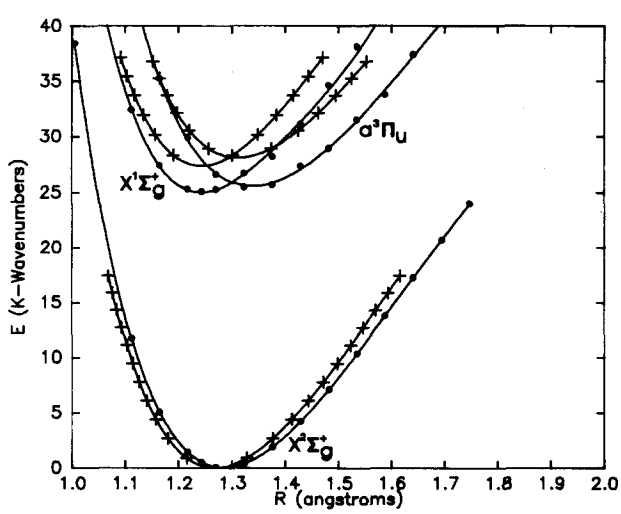

FIG. 2. Experimental (+) and theoretical (·) potential energy curves of the MCSCF $C_2^-\ X\,^2\Sigma_g^+$ and the MCEP $C_2^-\ X\,^2\Sigma_g^+ \rightarrow C_2\ X\,^1\Sigma_g^+$ and $C_2^-\ X\,^2\Sigma_g^+ \rightarrow C_2\ a\,^3\Pi_u$ states.

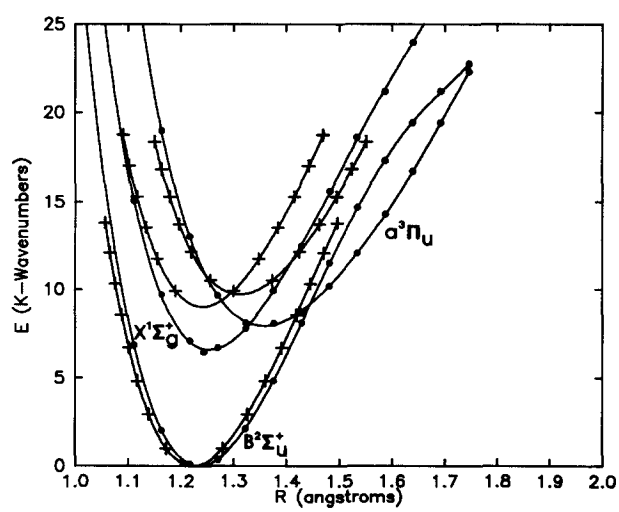

FIG. 3. Experimental (+) and calculated (·) potential energy curves of the MCSCF $C_2^-\ B\,^2\Sigma_u^+$ and the MCEP $C_2^-\ B\,^2\Sigma_u^+ \rightarrow C_2\ X\,^1\Sigma_g^+$ and $C_2^-\ B\,^2\Sigma_u^+ \rightarrow C_2\ a\,^3\Pi_u$ states.

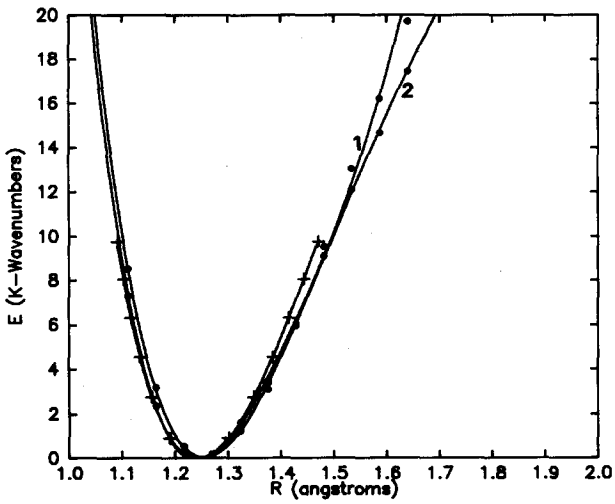

FIG. 4. The MCEP-computed C_2 $X\,^1\Sigma_g^+$ state determined from (1) the C_2^- $X\,^2\Sigma_g^+$ MCSCF reference state and (2) the C_2^- $B\,^2\Sigma_u^+$ MCSCF reference state. The + marks indicate the corresponding experimental curve and identify its vibrational levels.

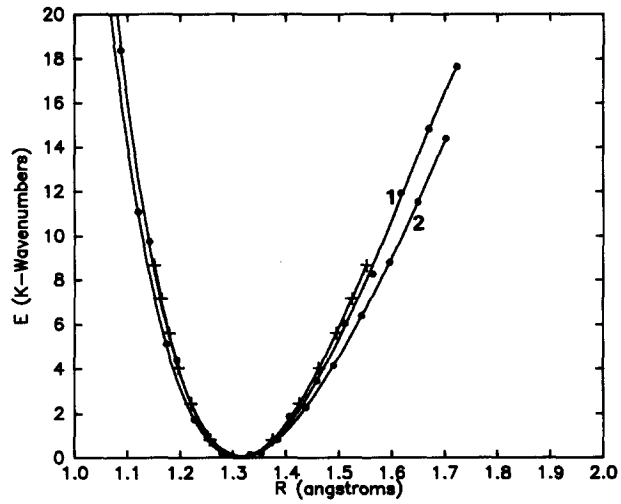

FIG. 6. The MCEP-computed C_2 $a\,^3\Pi_u$ state determined from (1) the C_2^- $X\,^2\Sigma_g^+$ MCSCF reference state and (2) the C_2^- $B\,^2\Sigma_u^+$ MCSCF reference state. R-shifted to superimpose the minima onto the experimental curve minimum. The + marks indicate the experimental curve and identify its vibrational levels.

of-the-art calculations, are common and entirely within the range of our expectations. Based upon the earlier work of Dupuis and Liu, described in Sec. I B, we expect that C_2^- should be *less* correlated than C_2. If so, one would expect that a given level of calculation in C_2 and C_2^- should *over*estimate the splitting between the C_2 and C_2^- energies. We find just the opposite; we *under*estimate this splitting. Although it is not possible to say with certainty whether we are undercorrelating C_2^- or overcorrelating C_2, it is our belief, based on past experience, that our C_2^- energies are undercorrelated.

(iii) The fact that the same 0.3 eV shift is needed to force the C_2 potentials derived by adding MCEP detachment energies to either our C_2^- $X\,^2\Sigma_g^+$ or to our $B\,^2\Sigma_u^+$ reference potentials indicates that our two C_2^- potentials are accurate (i.e., compare well to experimental data) and that our MCEP method is very robust. The robustness is demonstrated by the fact that the MCEP method treats equally well the simple orbital ionizations involved in the $X\,^2\Sigma_g^+$ to $X\,^1\Sigma_g^+$ and $a\,^3\Pi_u$ ionizations as well as the shakeup ionizations which connect the $B\,^2\Sigma_u^+$ state to $X\,^1\Sigma_g^+$ and $a\,^3\Pi_u$.

B. Autoionization of $B\,^2\Sigma_u^+$

Although most of our theoretical data is in excellent agreement with what is known from experiment, our $a\,^3\Pi_u$

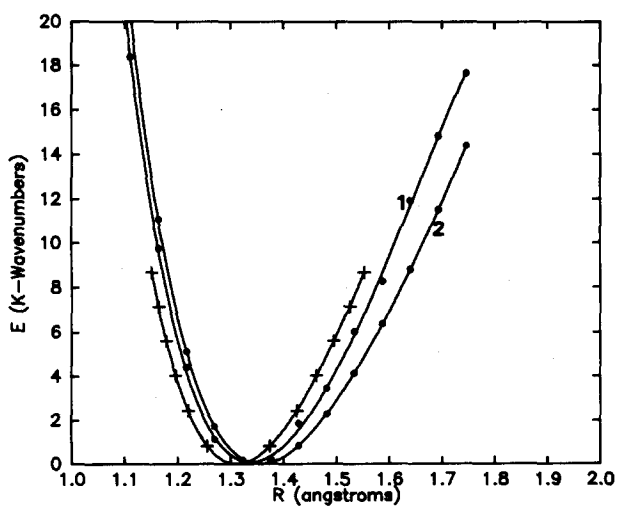

FIG. 5. The MCEP-computed C_2 $a\,^3\Pi_u$ state determined from (1) the C_2^- $X\,^2\Sigma_g^+$ MCSCF reference state and (2) the C_2^- $B\,^2\Sigma_u^+$ MCSCF reference state. The + marks indicate the corresponding experimental curve and identify vibrational levels.

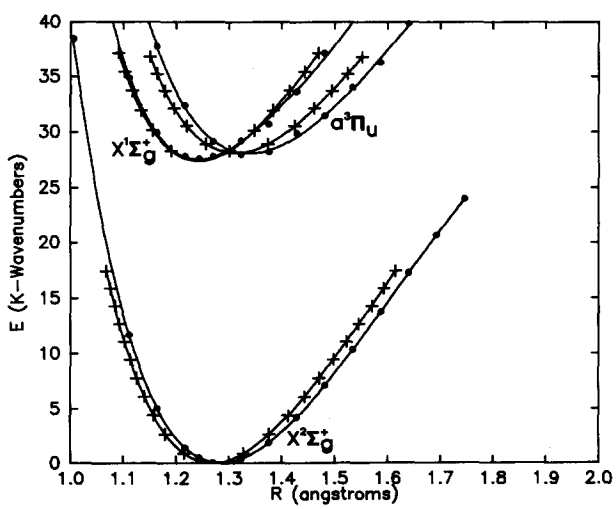

FIG. 7. Experimental and calculated potential energy curves of the MCSCF C_2^- $X\,^2\Sigma_g^+$ state and the MCEP C_2^- $X\,^2\Sigma_g^+ \rightarrow C_2$ $X\,^1\Sigma_g^+$ and C_2^- $X\,^2\Sigma_g^+ \rightarrow C_2$ $a\,^3\Pi_u$ states energy-shifted 2.5 k cm^{-1}. The + marks indicate the corresponding experimental curves and identify its vibrational levels.

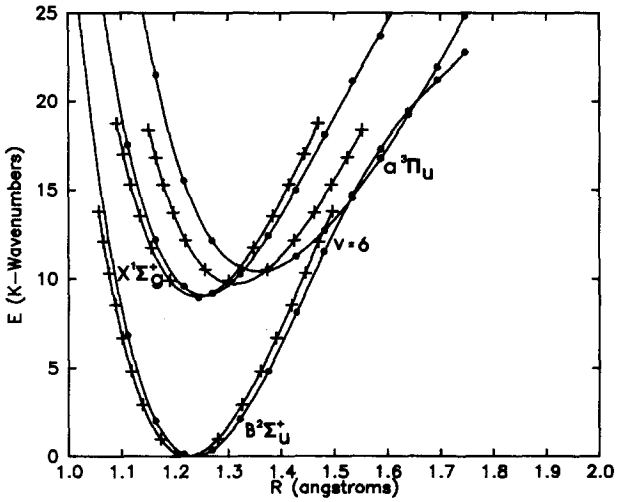

FIG. 8. Experimental and calculated potential energy curves of the MCSCF C_2^- $B\,^2\Sigma_u^+$ state and the MCEP C_2^- $B\,^2\Sigma_u^+ \rightarrow C_2\,X\,^1\Sigma_g^+$ and C_2^- $B\,^2\Sigma_u^+ \rightarrow C_2\,a\,^3\Pi_u$ states energy-shifted 2.5 k cm^{-1}. The + marks indicate the corresponding experimental curves and identify the vibrational levels.

potential and, in particular, the relative positioning of the neutral $a\,^3\Pi_u$ and anion $B\,^2\Sigma_u^+$ curves do not seem to agree well with the experimental information[7] (see Fig. 8). It is especially perplexing that our $B\,^2\Sigma_u^+$ and $a\,^3\Pi_u$ potentials approach closely and may even intersect at energies near the $v = 6$ vibrational level of the $B\,^2\Sigma_u^+$ state.

Recall that Jones *et al.*[7] observed a sudden tenfold increase in the autodetachment rate of C_2^- $B\,^2\Sigma_u^+$ in going from the $v = 5$ to the $v = 6$ level. They interpreted this result to mean that the $v = 5$ level of $B\,^2\Sigma_u^+$ C_2^- lies above $v = 0$ of $X\,^1\Sigma_g^+$ C_2 but below $v = 0$ of $a\,^3\Pi_u$, whereas $v = 6$ $B\,^2\Sigma_u^+$ C_2^- lies above $v = 0$ of $a\,^3\Pi_u$. Thus, at $v = 6$ the $a\,^3\Pi_u$ state becomes energetically accessible, and the rate of autodetachment could therefore be expected to increase due to the new open decay channel.

Why should there be a tenfold increase in decay rate in going from the $v = 5$ to the $v = 6$ levels of $B\,^2\Sigma_u^+$? As Table I clearly illustrates, and Jones *et al.* correctly argue, decay from $B\,^2\Sigma_u^+$ to $X\,^1\Sigma_g^+$ (which is predominantly $2\sigma_u^2 1\pi_u^4$) plus an ejected electron involves a two-electron event with respect to either of the two most important electronic configurations (the $2\sigma_u^1 1\pi_u^4 3\sigma_g^2$ or the $2\sigma_u^2 1\pi_u^3 3\sigma_g^1 n\pi_g^1$) of $B\,^2\Sigma_u^+$ (see Table I). In contrast, decay from $B\,^2\Sigma_u^+$ to $a\,^3\Pi_u$ (which is predominantly $2\sigma_u^2 1\pi_u^3 3\sigma_g^1$) can occur via a one-electron process from the $2\sigma_u^2 1\pi_u^3 3\sigma_g^1 n\pi_g^1$ configuration which contributes strongly to the $B\,^2\Sigma_u^+$ state at $R > 1.5$ Å.

It is therefore possible that differences in the electronic configuration composition of the $X\,^1\Sigma_g^+$ and $a\,^3\Pi_u$ state, combined with the opening of the $a\,^3\Pi_u$ manifold at $v = 6$ of $B\,^2\Sigma_u^+$, are the source of the tenfold rate difference between the $v = 5$ and $v = 6$ levels of $B\,^2\Sigma_u^+$ C_2^-. However, we wish to point out that *both* decay processes (to the $X\,^1\Sigma_g^+$ or to the $a\,^3\Pi_u$) require, in the picture of Jones *et al.*, nonadiabatic mixing because the $B\,^2\Sigma_u^+$ potential energy curve crosses neither the $X\,^1\Sigma_g^+$ nor the $a\,^3\Pi_u$ curve.

Jones *et al.*[7] also argue that the tenfold rate difference may be related to differences in the vibrational quantum number changes Δv which accompany the $B\,^2\Sigma_u^+$ $v = 5 \rightarrow X\,^1\Sigma_g^+ + e$ and the $B\,^2\Sigma_u^+$ $v = 6 \rightarrow X\,^1\Sigma_g^+ + e$ or $a\,^3\Pi_u + e$ processes. After considering all of the information available to us, including our own potential curves, it is our opinion that:

(i) The most likely source of the large decay-rate difference for $v = 5$ and $v = 6$ $B\,^2\Sigma_u^+$ C_2^- is the two-electron vs one-electron nature of the electronic processes which arise (both occurring via nonadiabatic or vibronic coupling).

(ii) The Δv propensities discussed by Jones *et al.* are likely not relevant because they were obtained (by Berry[22]) for autoionization of Rydberg states of H_2 in which the potential curves of the Rydberg and cation states are nearly identical. The $B\,^2\Sigma_u^+$ curve is not "parallel" to either the $X\,^1\Sigma_g^+$ or the $a\,^3\Pi_u$ curve, so the analogy is questionable.

(iii) Our calculated $B\,^2\Sigma_u^+$ and $a\,^3\Pi_u$ potential curves indicate that these two states may actually cross near $R = 1.55$ Å. Although our basis set and treatment of electron correlation effects are reasonably good, we do not feel confident in claiming that these curves do cross, but we think it worthwhile to stress this possibility. If these two curves were to cross, then $v = 6$ $B\,^2\Sigma_u^+$ could sample bond lengths near $R = 1.55$ Å and thereby undergo purely electronic one-electron autoionization via ejection of the $n\pi_g$ electron from

TABLE III. MCSCF total energies and large CSF amplitudes (C_i^2) for the C_2^- $X\,^2\Sigma_g^+$ and C_2^- $B\,^2\Sigma_u^+$ states.

Internuclear distance R	1.9 bohr (1.005 Å)	2.1 (1.111)	2.3 (1.217)	2.5 (1.323)	2.7 (1.429)	2.9 (1.535)	3.1 (1.640)	3.3 (1.746)
$X\,^2\Sigma_g^+$ Total energy (a.u.)	−75.501 439	−75.623 402	−75.670 302	−75.675 107	−75.657 607	−75.629 665	−75.598 272	−75.567 371
$2\sigma_u^2\pi_u^4 3\sigma_g^1$	0.91	0.90	0.80	0.66	0.54	0.43	0.35	0.28
$\pi_u^4\,{}^3(3\sigma_u^1 3\sigma_g^1)2\sigma_u^1$	0.02	0.00	0.06	0.13	0.19	0.23	0.26	0.26
$\pi_u^4\,{}^1(3\sigma_u^1 3\sigma_g^1)2\sigma_u^1$	0.00	0.01	0.05	0.09	0.12	0.14	0.16	0.16
$\pi_u^4 3\sigma_u^2 3\sigma_g^1$	0.00	0.00	0.00	0.01	0.03	0.06	0.09	0.11
$B\,^2\Sigma_u^+$ Total energy (a.u.)	−75.446 291	−75.551 008	−75.581 707	−75.572 657	−75.545 314	−75.515 336	−75.493 675	−75.478 477
$2\sigma_u^1\pi_u^4 3\sigma_g^2$	0.90	0.88	0.80	0.68	0.52	0.31	0.12	0.05
$\pi_u^4 3\sigma_g^2 3\sigma_u^1$	0.01	0.00	0.04	0.09	0.13	0.12	0.07	0.04
$2\sigma_u^2\pi_{ux}^3\,{}^1(3\sigma_g^1\pi_{uy}^1)\pi_{gy}^1$	0.02	0.03	0.05	0.06	0.08	0.11	0.11	0.10
$2\sigma_u^2\pi_{uy}^3\,{}^1(3\sigma_g^1\pi_{ux}^1)\pi_{gx}^1$	0.02	0.03	0.05	0.06	0.08	0.11	0.11	0.10
$\pi_{ux}^2\,{}^1({}^1(3\sigma_u^1 3\sigma_g^1)2\sigma_u^1)\pi_{uy}^1)\pi_{gy}^1$	0.00	0.00	0.00	0.01	0.03	0.06	0.09	0.10
$\pi_{uy}^2\,{}^1({}^1({}^3(3\sigma_u^1 3\sigma_g^1)2\sigma_u^1)\pi_{ux}^1)\pi_{gx}^1$	0.00	0.00	0.00	0.01	0.03	0.06	0.09	0.10
$\pi_{ux}^2\,{}^1({}^3({}^1(3\sigma_u^1 3\sigma_g^1)2\sigma_u^1)\pi_{uy}^1)\pi_{gy}^1$	0.00	0.00	0.00	0.00	0.01	0.03	0.06	0.07
$\pi_{uy}^2\,{}^1({}^3({}^1(3\sigma_u^1 3\sigma_g^1)2\sigma_u^1)\pi_{ux}^1)\pi_{gx}^1$	0.00	0.00	0.00	0.00	0.01	0.03	0.06	0.07

TABLE IV. MCEP ionization energies and corresponding important probabilities N_i for the $C_2^-\ X\,^2\Sigma_g^+ \rightarrow C_2\ X\,^1\Sigma_g^+ + e$ and $C_2^-\ X\,^2\Sigma_g^+ \rightarrow C_2\ a\,^3\Pi_u + e$ transitions.

Internuclear distance R	1.9 bohr (1.005 Å)	2.1 (1.111)	2.3 (1.217)	2.5 (1.323)	2.7 (1.429)	2.9 (1.535)	3.1 (1.640)	3.3 (1.746)
$X\,^2\Sigma_g^+ \rightarrow X\,^1\Sigma_g^+$ (eV)	2.065	2.567	2.966	3.269	3.342	3.450	3.422	4.058
$d_{3\sigma_g}$	0.64	0.71	0.76	0.78	0.78	0.73	0.51	0.64
$d_{2\sigma_g}$	0.01	0.01	0.01	0.02	0.01	0.01	0.01	0.01
$X\,^2\Sigma_g^+ \rightarrow a\,^3\Pi_u$ (eV)	4.576	3.990	3.534	3.118	2.873	2.629	2.504	2.375
$u_{1\pi_u}$	0.96	0.96	0.96	0.96	0.95	0.94	0.93	0.92

the $2\sigma_u^2 1\pi_u^3 3\sigma_g^1 n\pi_g^1$ configuration of $B\,^2\Sigma_u^+$. The fact that vibronic coupling would *not* be required would then give rise to the large rate enhancement. Against this interpretation we offer the observation that the decay rates estimated by Jones *et al.* ($\sim 10^6$–$10^7\ s^{-1}$) lie within our experience base[23] for nonadiabatic-induced decay processes; in contrast, purely electronic decay usually occurs at much higher rates ($\sim 10^{12}\ s^{-1}$ or faster).

C. Ion–neutral energy differences and equilibrium bond lengths

To assist other workers in reproducing and interpreting our results, we reproduce in Tables III–V a representative sample of our $X\,^2\Sigma_g^+$ and $B\,^2\Sigma_u^+$ MCSCF energies as well as our $X\,^1\Sigma_g^+$ and $a\,^3\Pi_u$ MCEP energies at several bond lengths ranging from 1.9 bohrs (1.005 Å) to 3.3 bohrs (1.746 Å). In Table III we include a listing of the dominant electronic configurations along with their weighting coefficients, for both the $X\,^2\Sigma_g^+$ and $B\,^2\Sigma_u^+$ MCSCF wave functions. Notice the strong variation of the $^2\Sigma_u^+$ state's mixing coefficients with bond length. In Tables IV and V, we also display the most important ionization operators and their N_i probability coefficients[15(a)] for ionizations to the $X\,^1\Sigma_g^+$ and $a\,^3\Pi_u$ states of C_2 from the $X\,^2\Sigma_g^+$ and $B\,^2\Sigma_u^+$ states of C_2^-, respectively. Note that ionizations from the $B\,^2\Sigma_u^+$ state are predominantly shakeup in nature (see Table V) whereas those from the $X\,^2\Sigma_g^+$ state are predominantly single-orbital ionizations (see Table IV).

Least-squares polynomial fits to each of the above potentials evaluated at 15 bond lengths ranging between 1.9 and 3.3 bohrs were used to obtain the energies at the minima in these potentials and the equilibrium bond lengths for each state. These quantities are compared to experimental results for each of the six curves in Table VI. Best polynomial fits up to tenth order resulted in an average standard deviation for all of the curves of 120 cm^{-1}. These "bottom-of-the-well" energies were then used to calculate T_e values for the anion-to-neutral species transitions setting $T_e = 0$ for $X\,^2\Sigma_g^+\ C_2^-$. An experimental T_e for $X\,^1\Sigma_g^+\ C_2$ can be obtained from an adiabatic electron affinity simply by taking into account any difference between the zero-point vibrational levels of the two species. A comparison of our computed and experimentally inferred T_e values is given in Table VII.

As Table VI shows, the equilibrium bond lengths obtained from our calculated energies are in reasonably good agreement with what is known from experiment.[24] The largest discrepancy is in the $a\,^3\Pi_u$ state of C_2. The ion–neutral energy differences shown in Table VII clearly illustrate that if both of our anion state energies are shifted downward in energy by approximately 0.3 eV, we achieve excellent agreement with the energy differences inferred from experimental data.[24] We pointed out this need for a 0.3 eV energy shift earlier in Sec. III A where we also explained that such errors in theoretically calculated EAs are quite common and to be expected. Quite frankly, we believe that, once this single 0.3 eV shift is introduced, all of our anion and neutral potential energy curves provide reliable and accurate representations of the true surfaces.

In order to explore the other low-lying C_2 neutral states, we used $C_2^-\ X\,^2\Sigma_g^+$ as a MCSCF reference state at its equilibrium bond length 2.40 bohr (1.270 Å) and calculated the entire MCEP vertical detachment energy (DE) spectrum.

TABLE V. MCEP ionization energies and corresponding important probabilities N_i for the $C_2^-\ B\,^2\Sigma_u^+ \rightarrow C_2\ X\,^1\Sigma_g^+ + e$ and $C_2^-\ B\,^2\Sigma_u^+ \rightarrow C_2\ a\,^3\Pi_u + e$ transitions.

Internuclear distance R	1.9 bohr (1.005 Å)	2.1 (1.111)	2.3 (1.217)	2.5 (1.323)	2.7 (1.429)	2.9 (1.535)	3.1 (1.640)	3.3 (1.746)
$B\,^2\Sigma_u^+ \rightarrow X\,^1\Sigma_g^+$ (eV)	1.133	1.018	0.864	0.702	0.543	0.488	0.563	0.779
$d_{2\sigma_u}$	0.32	0.24	0.17	0.11	0.07	0.03	0.00	0.00
$d_{3\sigma_u}$	0.00	0.01	0.02	0.04	0.05	0.04	0.02	0.01
$d_{1\pi_g}\,\lvert^2\Pi_g\rangle\langle 0\rvert$	0.92	0.92	0.90	0.83	0.75	0.84	0.85	0.81
$B\,^2\Sigma_u^+ \rightarrow a\,^3\Pi_u$ (eV)	3.875	2.653	1.602	0.743	0.080	−0.325	−0.336	−0.056
$u_{1\pi_g}$	0.00	0.00	0.00	0.00	0.00	0.02	0.05	0.08
$u_{1\pi_u}\,\lvert X\,^2\Sigma_g^+\rangle\langle 0\rvert$	0.95	0.96	0.97	0.97	0.97	0.98	0.97	0.97

TABLE VI. Equilibrium total energies and internuclear distances (R_e) for the calculated C_2^- $B\,^2\Sigma_u^+$, C_2 $X\,^1\Sigma_g^+$, and C_2 $a\,^3\Pi_u$ potential surfaces.

State	E (hartree)	R_e (bohr) Calculated	R_e (bohr) Experimental
$X\,^2\Sigma_g^+$ MCSCF	−75.6768	2.4278	2.3967
$B\,^2\Sigma_u^+$ MCSCF	−75.5823	2.3351	2.3119
$X\,^1\Sigma_g^+$ MCEP[a]	−75.5624	2.3398	2.3480
$a\,^3\Pi_u$ MCEP[a]	−75.5611	2.5226	2.4791
$X\,^1\Sigma_g^+$ MCEP[b]	−75.5524	2.3656	2.3480
$a\,^3\Pi_u$ MCEP[b]	−75.5462	2.5632	2.4791

[a] With $X\,^2\Sigma_g^+$ C_2^- as the MCSCF reference state (see the text).
[b] With $B\,^2\Sigma_u^+$ C_2^- as the MCSCF reference state.

The results for all DEs within 15 eV are given in Table VIII. To the best of our knowledge, no experimental data is available for direct comparison of most of these vertical DEs. A crude comparison to experimental data, which should bring out any especially interesting features of the DE spectrum, can be achieved by subtracting from our DEs the C_2^- $X\,^2\Sigma_g^+ \rightarrow C_2\,X\,^1\Sigma_g^+$ vertical DE. This, in essence, transforms our C_2^- $X\,^2\Sigma_g^+$ vertical DE spectrum into a $C_2\,X\,^1\Sigma_g^+$ vertical ($R = 2.40$ bohr; 1.270 Å) electronic excitation spectrum. We can then compare these vertical excitations to experimental T_e values[24] realizing, of course, that any vertical excitation will be *greater* than the corresponding T_e value. It should also be noted that the experimental R_e for each of these known states is given in Table VIII and that the greater the difference in that state's R_e and the $C_2\,X\,^1\Sigma_g^+$ state's R_e $R = 2.40$ bohr (1.270 Å), the greater the difference should be between our excitation energies and the correct T_e values. Examining Table VIII, it is apparent that most of our calculated vertical excitation energies are located as expected. Two states for which this is not true are the $^3\Sigma_u^+$ state with a calculated vertical excitation energy of 0.83 eV and an experimental T_e of 1.65 eV and the $^3\Pi_g$ state with a calculated vertical excitation energy of 2.15 eV and an experimental T_e of 2.48 eV. It should be noted that the information used to experimentally characterize the $^3\Sigma_u^+$ state involved perturbations[24] in the $A\,^1\Pi_u$ state of C_2. A great deal of work[12] has been done with the C_2 $d\,^3\Pi_g \rightarrow a\,^3\Pi_u$ Swan system both experimentally and theoretically. The experimental 0–0 line is at 2.40 eV and this would therefore indicate that our $^3\Pi_g$ IP is too low by 0.3–0.4 eV. In any event, our "broad brush stroke" vertical spectrum clearly identifies several well-known states and indicates that there may be several other, yet undetected, excited states of C_2 in the 0–11 eV energy range.

TABLE VII. Calculated and experimental ion–neutral energy differences (comparing "bottom-of-well" to "bottom-of-well" or T_e values).

Transition	MCEP	Experimental T_e[a]
$X\,^1\Sigma_g^+$ $C_2 \rightarrow X\,^2\Sigma_g^+$ C_2^-	3.112 eV	3.370–3.404 eV
$a\,^3\Pi_u$ $C_2 \rightarrow X\,^2\Sigma_g^+$ C_2^-	3.147 eV	3.459–3.493 eV
$X\,^1\Sigma_g^+$ $C_2 \rightarrow B\,^2\Sigma_u^+$ C_2^-	0.8133 eV	1.090–1.124 eV
$a\,^3\Pi_u$ $C_2 \rightarrow B\,^2\Sigma_u^+$ C_2^-	0.9819 eV	1.179–1.213 eV

[a] The comparable experimental T_e values were obtained by shifting the reported EA range of 3.374–3.408 by the appropriate $X\,^2\Sigma_g^+$ ($v = 0$) C_2^- and $X\,^1\Sigma_g^+$ ($v = 0$) C_2 vibrational energy difference of 0.004 eV.

TABLE VIII. MCEP-computed vibrational detachment energies (DE) $\leqslant$15.00 eV from the MCSCF $X\,^2\Sigma_g^+$ reference state at $R = 2.40$ bohr (1.270 Å).

State	DE (eV)	$-X\,^1\Sigma_g^+$ DE	Expt. T_e[a] (eV)	Expt. R_e (Å)
$^1\Sigma_g^+$	3.13	0	0	1.2425
$^3\Pi_u$	3.30	0.17 (−0.03)[b]	0.09	1.3119
$^3\Sigma_u^+$	3.96	0.83 (0.80)	1.65	1.23
$^3\Sigma_g^-$	4.54	1.41 (1.49)	0.80	1.3692
$^1\Pi_u$	4.62	1.49 (1.14)	1.04	1.3184
$^3\Pi_g$	5.28	2.15 (2.47)	2.48	1.2661
$^1\Delta_g$	5.36	2.23 (1.59)		
$^1\Sigma_g^+$	6.15	3.02 (1.81)		
$^1\Pi_g$	7.46	4.33 (4.81)	4.25	1.2552
$^1\Sigma_u^+$	9.32	6.19 (6.23)	5.36	1.2380
$^3\Sigma_u^+$	9.40	6.27		
$^3\Delta_u$	10.22	7.09		
$^3\Pi_g$	10.55	7.42	5.06	1.5351
$^1\Sigma_g^+$	10.81	7.68	6.82	1.2529
$^3\Sigma_u^-$	11.12	7.99		
$^1\Delta_u$	11.34	8.21		
$^3\Phi_g$	11.71	8.58		
$^3\Phi_g$	11.81	8.68		
$^3\Sigma_g^+$	11.82	8.69		
$^1\Sigma_u^-$	11.90	8.77		
$^1\Pi_g$	12.17	9.04		
$^3\Sigma_g^-$	12.30	9.17	8.81	1.393
$^1\Delta_u$	12.32	9.19		
$^3\Delta_u$	12.46	9.33		
$^3\Delta_g$	12.59	9.46	9.07	1.3579
$^3\Sigma_u^+$	12.61	9.48		
$^1\Phi_g$	12.64	9.51		
$^3\Pi_g$	12.73	9.60		
$^3\Pi_u$	13.01	9.88		
$^1\Pi_g$	13.65	10.52		
$^3\Pi_u$	13.71	10.58		
$^1\Sigma_g^+$	13.99	10.86		
$^3\Delta_g$	14.03	10.90		
$^3\Sigma_g^-$	14.14	11.01		

[a] These are "bottom-of-the-well" T_e taken with respect to $C_2\,X\,^1\Sigma_g^+$ (see Ref. 24).
[b] Other theoretical CI (adiabatic) energies of K. Kirby and B. Liu, J. Chem. Phys. 70, 893 (1979).

D. Concluding remarks

Using the MCSCF-MCEP computational method, we have examined primarily the $X\,^2\Sigma_g^+$ and $B\,^2\Sigma_u^+$ states of C_2^- and the $X\,^1\Sigma_g^+$ and $a\,^3\Pi_u$ states of C_2. After incorporating a single common systematic shift in our anion-to-neutral energy differences of 0.3 eV, our potential energy curves for these four states seem to agree well with what is known experimentally except, perhaps, for the *relative* positioning of the $B\,^2\Sigma_u^+$ and $a\,^3\Pi_u$ curves. Possible implications of these differences for the autoionization mechanism of vibrationally excited $B\,^2\Sigma_u^+$ C_2^- are discussed, and the possibility of a curve crossing is addressed.

Having established the value of our computational tools by reproducing known experimental data of this very diffi-

cult C_2/C_2^- system, we examined the *vertical* electronic detachment spectrum of C_2^- in an attempt to qualitatively identify all low-lying (0–11 eV) excited states of C_2. This "broad brush stroke" investigation was intended not to accurately determine excitation energies of C_2 (which cannot be obtained from a vertical spectrum) but to look for new excited states of C_2. In addition to identifying 12 known states of C_2, we predict 22 other states.

ACKNOWLEDGMENTS

We acknowledge the financial support of the National Science Foundation (CHE-8511307), the U.S. Army Research Office (DAAG-2984K0086), and the donors of the Petroleum Research Fund, administered by the American Chemical Society (PRF14446AC6). We also acknowledge the Harris Corporation for their generous computer system grant.

[1]R. R. Corderman and W. C. Lineberger, Annu. Rev. Phys. Chem. **30**, 347 (1979).
[2]G. Herzberg and A. Lagerqvist, Can. J. Phys. **46**, 2363 (1968)
[3]R. D. Mead, U. Hefter, P. A. Schulz, and W. C. Lineberger, J. Chem. Phys. **82**, 1723 (1985).
[4]W. C. Lineberger and T. A. Patterson, Chem. Phys. Lett. **13**, 40 (1972).
[5]M. Zeitz, S. D. Peyerimhoff, and R. J. Buenker, Chem. Phys. Lett. **64**, 243 (1979).
[6]D. Feldman, Z. Naturforsch. Teil A **25**, 621 (1970).
[7]P. L. Jones, R. D. Mead, B. E. Kohler, S. D. Rosner, and W. C. Lineberger, J. Chem. Phys. **73**, 4419 (1980).
[8]M. Dupuis and B. Liu, J. Chem. Phys. **73**, 337 (1980).
[9]P. L. Jones, Ph.D. thesis, University of Colorado, 1980.
[10]P. E. Cade and A. C. Wahl, At. Data Nucl. Tables **13**, 339 (1974).
[11]J. Barsuhn, J. Phys. B **7**, 155 (1974).
[12]M. Zeitz, S. D. Peyerimhoff, and R. J. Buenker, Chem. Phys. Lett. **58**, 487 (1978).
[13]P. Rosmus and H. Werner, J. Chem. Phys. **80**, 5085 (1984).
[14]L. S. Cederbaum, W. Domcke, and W. von Niessen, J. Phys. B **10**, 2963 (1977).
[15](a) J. A. Nichols, D. L. Yeager, and P. Jørgensen, J. Chem. Phys. **80**, 293 (1984); (b) J. T. Golab, B. S. Thies, D. L. Yeager, and J. A. Nichols, *ibid.* **84**, 284 (1986).
[16]J. Linderberg and Y. Öhrn, *Propagators in Quantum Chemistry* (Academic, London, 1973).
[17]B. T. Pickup and A. Mukhopadhyay, Chem. Phys. Lett. **79**, 109 (1981).
[18]I. Shavitt, in *Modern Theoretical Chemistry*, edited by H. F. Schaefer III (Plenum, New York, 1977), Vol. 3.
[19]T. H. Dunning, Jr., J. Chem. Phys. **55**, 716 (1971).
[20]B. Roos and P. Siegbahn, Theor. Chim. Acta **17**, 199 (1970).
[21]T. H. Dunning and P. J. Hay, in *Modern Theoretical Chemistry*, edited by H. F. Schaefer III (Plenum, New York, 1977), Vol. 3.
[22]R. S. Berry, J. Chem. Phys. **45**, 1228 (1966).
[23](a) P. K. Acharya, R. A. Kendall, and J. Simons, J. Am. Chem. Soc. **106**, 3402 (1984); (b) J. Chem. Phys. **83**, 3888 (1985).
[24]K. P. Huber and G. Herzberg, *Constants of Diatomic Molecules* (Van Nostrand, New York, 1979).